The Astrophysical Journal, 984:123 (11pp), 2025 May 9 https://doi.org/10.3847/1538-4357/adbdc5

The Distribution of Ultrahigh-energy Cosmic Rays along the Supergalactic Plane Measured at the Pierre Auger Observatory

A. Abdul Halim[1], P. Abreu[2], M. Aglietta[3,4], I. Allekotte[5], K. Almeida Cheminant[6], A. Almela[7,8], R. Aloisio[9,10], J. Alvarez-Muñiz[11], J. Ammerman Yebra[11], G.A. Anastasi[3,4], L. Anchordoqui[12], B. Andrada[7], S. Andringa[2], Anukriti[13], L. Apollonio[14,15], C. Aramo[16], P.R. Araújo Ferreira[17], E. Arnone[3,18], J.C. Arteaga Velázquez[19], P. Assis[2], G. Avila[20], E. Avocone[10,21], A. Bakalova[22], F. Barbato[9,10], A. Bartz Mocellin[23], J.A. Bellido[1,24], C. Berat[25], M.E. Bertaina[3,18], G. Bhatta[6], M. Bianciotto[3,18], P.L. Biermann[100], V. Binet[26], K. Bismark[7,27], T. Bister[28,29], J. Biteau[30,93], J. Blazek[22], C. Bleve[25], J. Blümer[31], M. Boháčová[22], D. Boncioli[10,21], C. Bonifazi[32,33], L. Bonneau Arbeletche[34], N. Borodai[6], J. Brack[102], P.G. Brichetto Orchera[7], F.L. Briechle[17], A. Bueno[35], S. Buitink[36], M. Buscemi[37,38], M. Büsken[7,27], A. Bwembya[28,29], K.S. Caballero-Mora[39], S. Cabana-Freire[11], L. Caccianiga[14,15], R. Caruso[37,40], A. Castellina[3,4], F. Catalani[41], G. Cataldi[42], L. Cazon[11], M. Cerda[43], A. Cermenati[9,10], J.A. Chinellato[34], J. Chudoba[22], L. Chytka[44], R.W. Clay[1], A.C. Cobos Cerutti[45], R. Colalillo[16,46], A. Coleman[47], M.R. Coluccia[42], R. Conceição[2], A. Condorelli[30], G. Consolati[14,48], M. Conte[42,49], F. Convenga[10,21], D. Correia dos Santos[50], P.J. Costa[2], C.E. Covault[51], M. Cristinziani[52], C.S. Cruz Sanchez[53], S. Dasso[54,55], K. Daumiller[31], B.R. Dawson[1], R.M. de Almeida[50], J. de Jesús[7,31], S.J. de Jong[28,29], J.R.T. de Mello Neto[33,56], I. De Mitri[9,10], J. de Oliveira[57], D. de Oliveira Franco[34], F. de Palma[42,49], V. de Souza[58], B.P. de Souza de Errico[33], E. De Vito[42,49], A. Del Popolo[37,40], O. Deligny[59], N. Denner[22], L. Deval[7,31], A. di Matteo[3], M. Dobre[60], C. Dobrigkeit[34], J.C. D'Olivo[61], L.M. Domingues Mendes[2], Q. Dorosti[52], J.C. dos Anjos[62], R.C. dos Anjos[63], J. Ebr[22], F. Ellwanger[31], M. Emam[28,29], R. Engel[27,31], I. Epicoco[42,49], M. Erdmann[17], A. Etchegoyen[7,8], C. Evoli[9,10], H. Falcke[28,29,64], J. Farmer[65], G. Farrar[66], A.C. Fauth[34], N. Fazzini[97], F. Feldbusch[67], F. Fenu[31,96], A. Fernandes[2], B. Fick[68], J.M. Figueira[7], A. Filipčič[13,69], T. Fitoussi[31], B. Flaggs[47], T. Fodran[28], T. Fujii[65,98], A. Fuster[7,8], C. Galea[28], C. Galelli[14,15], B. García[45], C. Gaudu[70], H. Gemmeke[67], F. Gesualdi[7,31], A. Gherghel-Lascu[60], P.L. Ghia[59], U. Giaccari[42], J. Glombitza[17,99], F. Gobbi[43], F. Gollan[7], G. Golup[5], M. Gómez Berisso[5], P.F. Gómez Vitale[20], J.P. Gongora[20], J.M. González[5], N. González[7], I. Goos[5], D. Góra[6], A. Gorgi[3,4], M. Gottowik[11], T.D. Grubb[1], F. Guarino[16,46], G.P. Guedes[71], E. Guido[52], L. Gülzow[31], S. Hahn[27], P. Hamal[22], M.R. Hampel[7], P. Hansen[53], D. Harari[5], V.M. Harvey[1], A. Haungs[31], T. Hebbeker[17], C. Hojvat[97], J.R. Hörandel[28,29], P. Horvath[44], M. Hrabovský[44], T. Huege[31,36], A. Insolia[37,40], P.G. Isar[72], P. Janecek[22], V. Jilek[22], J.A. Johnsen[23], J. Jurysek[22], K.-H. Kampert[70], B. Keilhauer[31], A. Khakurdikar[28], V.V. Kizakke Covilakam[7,31], H.O. Klages[31], M. Kleifges[67], F. Knapp[27], J. Köhler[31], N. Kunka[67], B.L. Lago[73], N. Langner[17], M.A. Leigui de Oliveira[74], Y. Lema-Capeans[11], A. Letessier-Selvon[75], I. Lhenry-Yvon[59], L. Lopes[2], L. Lu[76], Q. Luce[27], J.P. Lundquist[13], A. Machado Payeras[34], M. Majercakova[22], D. Mandat[22], B.C. Manning[1], P. Mantsch[97], S. Marafico[59], F.M. Mariani[14,15], A.G. Mariazzi[53], I.C. Mariş[77], G. Marsella[37,38], D. Martello[42,49], S. Martinelli[7,31], O. Martínez Bravo[78], M.A. Martins[11], H.-J. Mathes[31], J. Matthews[92], G. Matthiae[79,80], E. Mayotte[23,70], S. Mayotte[23], P.O. Mazur[97], G. Medina-Tanco[61], J. Meinert[70], D. Melo[7], A. Menshikov[67], C. Merx[31], S. Michal[44], M.I. Micheletti[26], L. Miramonti[14,15], S. Mollerach[5], F. Montanet[25], L. Morejon[70], C. Morello[3,4], K. Mulrey[28,29], R. Mussa[3], W.M. Namasaka[70], S. Negi[22], L. Nellen[61], K. Nguyen[68], G. Nicora[81], M. Niechciol[52], D. Nitz[68], D. Nosek[82], V. Novotny[82], L. Nožka[44], A. Nucita[42,49], L.A. Núñez[83], C. Oliveira[58], M. Palatka[22], J. Pallotta[81], S. Panja[22], G. Parente[11], T. Paulsen[70], J. Pawlowsky[70], M. Pech[22], J. Pekala[6], R. Pelayo[84], L.A.S. Pereira[85], E.E. Pereira Martins[7,27], J. Perez Armand[86], C. Pérez Bertolli[7,31], L. Perrone[42,49], S. Petrera[9,10], C. Petrucci[10,21], T. Pierog[31], M. Pimenta[2], M. Platino[7], B. Pont[28], M. Pothast[28,29], M. Pourmohammad Shahvar[37,38], P. Privitera[65], M. Prouza[22], A. Puyleart[68], S. Querchfeld[70], J. Rautenberg[70], D. Ravignani[7], J.V. Reginatto Akim[34], M. Reininghaus[27], J. Ridky[22], F. Riehn[11], M. Risse[52], V. Rizi[10,21], W. Rodrigues de Carvalho[28], E. Rodriguez[7,31], J. Rodriguez Rojo[20], M.J. Roncoroni[7], S. Rossoni[87], M. Roth[31], E. Roulet[5], A.C. Rovero[55], P. Ruehl[52], A. Saftoiu[60], M. Saharan[28], F. Salamida[10,21], H. Salazar[78], G. Salina[79], J.D. Sanabria Gomez[83], F. Sánchez[7], E.M. Santos[86], E. Santos[22], F. Sarazin[23], R. Sarmento[2], R. Sato[20], P. Savina[76], C.M. Schäfer[27], V. Scherini[42,49], H. Schieler[31], M. Schimassek[59], M. Schimp[70], D. Schmidt[31], O. Scholten[36,101], H. Schoorlemmer[28,29], P. Schovánek[22], F.G. Schröder[31,47], J. Schulte[17], T. Schulz[31], S.J. Sciutto[53], M. Scornavacche[7,31], A. Segreto[37,88], S. Sehgal[70], S.U. Shivashankara[13], G. Sigl[87], G. Silli[7], O. Sima[60,94], K. Simkova[36], F. Simon[67], R. Smau[60], R. Šmída[65], P. Sommers[103], J.F. Soriano[12], R. Squartini[43], M. Stadelmaier[14,15,31], S. Stanič[13], J. Stasielak[6], P. Stassi[25], S. Strähnz[27], M. Straub[17], T. Suomijärvi[30], A.D. Supanitsky[7], Z. Svozilikova[22], Z. Szadkowski[89], F. Tairli[1], A. Tapia[90], C. Taricco[3,18], C. Timmermans[28,29], O. Tkachenko[31], P. Tobiska[22], C.J. Todero Peixoto[41], B. Tomé[2], Z. Torrès[25], A. Travaini[43], P. Travnicek[22], C. Trimarelli[10,21], M. Tueros[53], M. Unger[31], L. Vaclavek[44], M. Vacula[44], J.F. Valdés Galicia[61], L. Valore[16,46], E. Varela[78], A. Vásquez-Ramírez[83], D. Veberič[31], C. Ventura[56], I.D. Vergara Quispe[53], V. Verzi[79], J. Vicha[22], J. Vink[91], S. Vorobiov[13], C. Watanabe[33], A.A. Watson[95], A. Weindl[31], L. Wiencke[23], H. Wilczyński[6], D. Wittkowski[70], B. Wundheiler[7], B. Yue[70], A. Yushkov[22], O. Zapparrata[77], E. Zas[11], D. Zavrtanik[13,69], M. Zavrtanik[13,69], and

The Pierre Auger Collaboration

[1] University of Adelaide, Adelaide, SA, Australia
[2] Laboratório de Instrumentação e Física Experimental de Partículas, LIP and Instituto Superior Técnico, IST, Universidade de Lisboa, UL, Lisboa, Portugal
[3] INFN, Sezione di Torino, Torino, Italy
[4] Osservatorio Astrofisico di Torino (INAF), Torino, Italy

[5] Centro Atómico Bariloche and Instituto Balseiro (CNEA-UNCuyo-CONICET), San Carlos de Bariloche, Argentina
[6] Institute of Nuclear Physics PAN, Krakow, Poland
[7] Instituto de Tecnologías en Detección y Astropartículas (CNEA, CONICET, UNSAM), Buenos Aires, Argentina
[8] Universidad Tecnológica Nacional, Facultad Regional Buenos Aires, Buenos Aires, Argentina
[9] Gran Sasso Science Institute, L'Aquila, Italy
[10] INFN Laboratori Nazionali del Gran Sasso, Assergi (L'Aquila), Italy
[11] Instituto Galego de Física de Altas Enerxías (IGFAE), Universidade de Santiago de Compostela, Santiago de Compostela, Spain
[12] Department of Physics and Astronomy, Lehman College, City University of New York, Bronx, NY, USA
[13] Center for Astrophysics and Cosmology (CAC), University of Nova Gorica, Nova Gorica, Slovenia
[14] INFN, Sezione di Milano, Milano, Italy
[15] Università di Milano, Dipartimento di Fisica, Milano, Italy
[16] INFN, Sezione di Napoli, Napoli, Italy
[17] RWTH Aachen University, III. Physikalisches Institut A, Aachen, Germany
[18] Università Torino, Dipartimento di Fisica, Torino, Italy
[19] Universidad Michoacana de San Nicolás de Hidalgo, Morelia, Michoacán, México
[20] Observatorio Pierre Auger and Comisión Nacional de Energía Atómica, Malargüe, Argentina
[21] Università dell'Aquila, Dipartimento di Scienze Fisiche e Chimiche, L'Aquila, Italy
[22] Institute of Physics of the Czech Academy of Sciences, Prague, Czech Republic
[23] Colorado School of Mines, Golden, CO, USA
[24] Universidad Nacional de San Agustin de Arequipa, Facultad de Ciencias Naturales y Formales, Arequipa, Peru
[25] Univ.Grenoble Alpes, CNRS, Grenoble Institute of Engineering Univ. Grenoble Alpes, LPSC-IN2P3, 38000 Grenoble, France
[26] Instituto de Física de Rosario (IFIR), CONICET/U.N.R. and Facultad de Ciencias Bioquímicas y Farmacéuticas U.N.R., Rosario, Argentina
[27] Karlsruhe Institute of Technology (KIT), Institute for Experimental Particle Physics, Karlsruhe, Germany
[28] IMAPP, Radboud University Nijmegen, Nijmegen, The Netherlands
[29] Nationaal Instituut voor Kernfysica en Hoge Energie Fysica (NIKHEF), Science Park, Amsterdam, The Netherlands
[30] Université Paris-Saclay, CNRS/IN2P3, IJCLab, Orsay, France
[31] Karlsruhe Institute of Technology (KIT), Institute for Astroparticle Physics, Karlsruhe, Germany
[32] International Center of Advanced Studies and Instituto de Ciencias Físicas, ECyT-UNSAM and CONICET, Campus Miguelete, San Martín, Buenos Aires, Argentina
[33] Universidade Federal do Rio de Janeiro, Instituto de Física, Rio de Janeiro, RJ, Brazil
[34] Universidade Estadual de Campinas, IFGW, Campinas, SP, Brazil
[35] Universidad de Granada and C.A.F.P.E., Granada, Spain
[36] Vrije Universiteit Brussels, Brussels, Belgium
[37] INFN, Sezione di Catania, Catania, Italy
[38] Università di Palermo, Dipartimento di Fisica e Chimica "E. Segrè," Palermo, Italy
[39] Universidad Autónoma de Chiapas, Tuxtla Gutiérrez, Chiapas, México
[40] Università di Catania, Dipartimento di Fisica e Astronomia "Ettore Majorana," Catania, Italy
[41] Universidade de São Paulo, Escola de Engenharia de Lorena, Lorena, SP, Brazil
[42] INFN, Sezione di Lecce, Lecce, Italy
[43] Observatorio Pierre Auger, Malargüe, Argentina
[44] Palacky University, Olomouc, Czech Republic
[45] Instituto de Tecnologías en Detección y Astropartículas (CNEA, CONICET, UNSAM), and Universidad Tecnológica Nacional, Facultad Regional Mendoza (CONICET/CNEA), Mendoza, Argentina
[46] Università di Napoli "Federico II," Dipartimento di Fisica "Ettore Pancini," Napoli, Italy
[47] University of Delaware, Department of Physics and Astronomy, Bartol Research Institute, Newark, DE, USA
[48] Politecnico di Milano, Dipartimento di Scienze e Tecnologie Aerospaziali, Milano, Italy
[49] Università del Salento, Dipartimento di Matematica e Fisica "E. De Giorgi," Lecce, Italy
[50] Universidade Federal Fluminense, EEIMVR, Volta Redonda, RJ, Brazil
[51] Case Western Reserve University, Cleveland, OH, USA
[52] Universität Siegen, Department Physik, Experimentelle Teilchenphysik, Siegen, Germany
[53] IFLP, Universidad Nacional de La Plata and CONICET, La Plata, Argentina
[54] Departamento de Física and Departamento de Ciencias de la Atmósfera y los Océanos, FCEyN, Universidad de Buenos Aires and CONICET, Buenos Aires, Argentina
[55] Instituto de Astronomía y Física del Espacio (IAFE, CONICET-UBA), Buenos Aires, Argentina
[56] Universidade Federal do Rio de Janeiro (UFRJ), Observatório do Valongo, Rio de Janeiro, RJ, Brazil
[57] Instituto Federal de Educação, Ciência e Tecnologia do Rio de Janeiro (IFRJ), Brazil
[58] Universidade de São Paulo, Instituto de Física de São Carlos, São Carlos, SP, Brazil
[59] CNRS/IN2P3, IJCLab, Université Paris-Saclay, Orsay, France
[60] "Horia Hulubei" National Institute for Physics and Nuclear Engineering, Bucharest-Magurele, Romania
[61] Universidad Nacional Autónoma de México, México, DF, México
[62] Centro Brasileiro de Pesquisas Fisicas, Rio de Janeiro, RJ, Brazil
[63] Universidade Federal do Paraná, Setor Palotina, Palotina, Brazil
[64] Stichting Astronomisch Onderzoek in Nederland (ASTRON), Dwingeloo, The Netherlands
[65] University of Chicago, Enrico Fermi Institute, Chicago, IL, USA
[66] New York University, New York, NY, USA
[67] Karlsruhe Institute of Technology (KIT), Institut für Prozessdatenverarbeitung und Elektronik, Karlsruhe, Germany
[68] Michigan Technological University, Houghton, MI, USA
[69] Experimental Particle Physics Department, J.Stefan Institute, Ljubljana, Slovenia
[70] Bergische Universität Wuppertal, Department of Physics, Wuppertal, Germany
[71] Universidade Estadual de Feira de Santana, Feira de Santana, Brazil
[72] Institute of Space Science, Bucharest-Magurele, Romania
[73] Centro Federal de Educação Tecnológica Celso Suckow da Fonseca, Petropolis, Brazil
[74] Universidade Federal do ABC, Santo André, SP, Brazil
[75] Laboratoire de Physique Nucléaire et de Hautes Energies (LPNHE), Sorbonne Université, Université de Paris, CNRS-IN2P3, Paris, France
[76] University of Wisconsin-Madison, Department of Physics and WIPAC, Madison, WI, USA
[77] Université Libre de Bruxelles (ULB), Brussels, Belgium

[78] Benemérita Universidad Autónoma de Puebla, Puebla, México
[79] INFN, Sezione di Roma "Tor Vergata," Roma, Italy
[80] Università di Roma "Tor Vergata," Dipartimento di Fisica, Roma, Italy
[81] Laboratorio Atmósfera, Departamento de Investigaciones en Láseres y sus Aplicaciones, UNIDEF (CITEDEF-CONICET), Argentina
[82] Charles University, Faculty of Mathematics and Physics, Institute of Particle and Nuclear Physics, Prague, Czech Republic
[83] Universidad Industrial de Santander, Bucaramanga, Colombia
[84] Unidad Profesional Interdisciplinaria en Ingeniería y Tecnologías Avanzadas del Instituto Politécnico Nacional (UPIITA-IPN), México, DF, México
[85] Universidade Federal de Campina Grande, Centro de Ciencias e Tecnologia, Campina Grande, Brazil
[86] Universidade de São Paulo, Instituto de Física, São Paulo, SP, Brazil
[87] Universität Hamburg, II. Institut für Theoretische Physik, Hamburg, Germany
[88] Istituto di Astrofisica Spaziale e Fisica Cosmica di Palermo (INAF), Palermo, Italy
[89] University of Łódź, Faculty of High-Energy Astrophysics, Łódź, Poland
[90] Universidad de Medellín, Medellín, Colombia
[91] Universiteit van Amsterdam, Faculty of Science, Amsterdam, The Netherlands
Received 2024 July 9; revised 2025 March 3; accepted 2025 March 4; published 2025 May 5

Abstract

Ultrahigh-energy cosmic rays are known to be mainly of extragalactic origin, and their propagation is limited by energy losses, so their arrival directions are expected to correlate with the large-scale structure of the local Universe. In this work, we investigate the possible presence of intermediate-scale excesses in the flux of the most energetic cosmic rays from the direction of the supergalactic plane region using events with energies above 20 EeV recorded with the surface detector array of the Pierre Auger Observatory up to 2022 December 31, with a total exposure of 135,000 km^2 sr yr. The strongest indication for an excess that we find, with a posttrial significance of 3.1σ, is in the Centaurus region, as in our previous reports, and it extends down to lower energies than previously studied. We do not find any strong hints of excesses from any other region of the supergalactic plane at the same angular scale. In particular, our results do not confirm the reports by the Telescope Array Collaboration of excesses from two regions in the Northern Hemisphere at the edge of the field of view of the Pierre Auger Observatory. With a comparable integrated exposure over these regions, our results there are in good agreement with the expectations from an isotropic distribution.

Unified Astronomy Thesaurus concepts: Cosmic rays (329); Ultra-high-energy cosmic radiation (1733); Cosmic anisotropy (316)

Materials only available in the online version of record: figure set

1. Introduction

The flux of ultrahigh-energy cosmic rays (UHECRs), atomic nuclei mainly of extragalactic origin reaching the Earth with energies $E \geqslant 1$ EeV $= 10^{18}$ eV ≈ 0.16 J each, is remarkably close to being the same from all directions in the sky, with the exception of a dipole moment in the celestial distribution of cosmic rays with $E \geqslant 8$ EeV (Pierre Auger Collaboration 2017, 2018a, 2020a) toward a direction $\sim$115° away from the Galactic center, with an amplitude of around 6% at 10 EeV and growing roughly linearly with energy. No anisotropies on intermediate or smaller angular scales have been conclusively discovered yet in data collected at either the Pierre Auger Observatory or the Telescope Array (TA), the two largest cosmic-ray detector arrays in the world (covering 3000 km^2 and 700 km^2, respectively), located in the Southern and Northern Hemispheres (latitudes $-35.2°$ and $+39.3°$), respectively. On the other hand, a few indications with statistical significances ranging from 3.0 to 4.6σ of such anisotropies in the flux of cosmic rays with more than a few tens of EeV have been reported. An excess of events in data from the Pierre Auger Observatory from a circular region on the celestial sphere centered on the Centaurus A (Cen A) radio galaxy, first reported in Pierre Auger Collaboration (2010), has reached a posttrial significance of 4.0σ (Pierre Auger Collaboration 2023). A correlation with the positions of nearby starburst galaxies first reported in Pierre Auger Collaboration (2018b), to which the main contributor is the NGC 4945 galaxy in the aforementioned Cen A region, has reached 3.8σ posttrial as of the last update (Pierre Auger Collaboration 2023). An analogous study combining data from both the Pierre Auger Observatory and the TA has reached 4.6σ posttrial (Pierre Auger Collaboration & Telescope Array Collaboration 2023b). Finally, the so-called "TA hotspot" at equatorial coordinates $(\alpha, \delta) \approx (145°, +40°)$ (Telescope Array Collaboration 2014) and a new excess at $(\alpha, \delta) \approx (20°, +35°)$ (Telescope Array Collaboration 2021b) in TA data have posttrial significances of around 3σ as of their last update (Telescope Array Collaboration 2023). All these regions where indications of excesses have been reported intersect the supergalactic plane (SGP), a great circle in the sky along which extragalactic matter within $\mathcal{O}(10^2$ Mpc) tends to be concentrated. The Local Sheet, a structure comprising nearly all bright galaxies within 6 Mpc (M. L. McCall 2014), is also remarkably aligned with the SGP. Hence, a concentration of the

[92] Louisiana State University, Baton Rouge, LA, USA.
[93] Institut universitaire de France (IUF), France.
[94] Also at University of Bucharest, Physics Department, Bucharest, Romania.
[95] School of Physics and Astronomy, University of Leeds, Leeds, UK.
[96] Now at Agenzia Spaziale Italiana (ASI). Via del Politecnico 00133, Roma, Italy.
[97] Fermi National Accelerator Laboratory, Fermilab, Batavia, IL, USA.
[98] Now at Graduate School of Science, Osaka Metropolitan University, Osaka, Japan.
[99] Now at ECAP, Erlangen, Germany.
[100] Max-Planck-Institut für Radioastronomie, Bonn, Germany.
[101] Also at Kapteyn Institute, University of Groningen, Groningen, The Netherlands.
[102] Colorado State University, Fort Collins, CO, USA.
[103] Pennsylvania State University, University Park, PA, USA.

Table 1
Information about the Maximum-significance Excesses Found along the SGP

		First Maximum								Second Maximum							
$E_{\min}$	N_{tot}	L	B	$\frac{\mathcal{E}_{\text{in}}}{\mathcal{E}_{\text{tot}}}$	N_{bg}	N_{in}	$\frac{\Phi_{\text{in}}}{\Phi_{\text{out}}}$	Z_{LM}	99% U.L.	L	B	$\frac{\mathcal{E}_{\text{in}}}{\mathcal{E}_{\text{tot}}}$	N_{bg}	N_{in}	$\frac{\Phi_{\text{in}}}{\Phi_{\text{out}}}$	Z_{LM}	99% U.L.
20 EeV	8832	162°	−6°	9.56%	829.	990	$1.19^{+0.04}_{-0.04}$	$+5.2\sigma$	1.29	241°	−5°	10.27%	900.	971	$1.08^{+0.04}_{-0.04}$	$+2.2\sigma$	1.17
25 EeV	5380	161°	−9°	9.56%	504.	608	$1.21^{+0.05}_{-0.05}$	$+4.2\sigma$	1.33	275°	−19°	8.00%	426.	482	$1.13^{+0.05}_{-0.05}$	$+2.6\sigma$	1.26
32 EeV	2936	163°	−8°	9.68%	276.	363	$1.32^{+0.08}_{-0.07}$	$+4.7\sigma$	1.50	276°	−17°	7.89%	229.	264	$1.15^{+0.08}_{-0.07}$	$+2.2\sigma$	1.34
40 EeV	1533	162°	−6°	9.56%	140.	208	$1.49^{+0.11}_{-0.11}$	$+5.1\sigma$	1.77	345°	−7°	1.00%	15.2	26	$1.71^{+0.36}_{-0.32}$	$+2.5\sigma$	2.68
50 EeV	713	161°	−7°	9.56%	64.4	103	$1.60^{+0.18}_{-0.16}$	$+4.2\sigma$	2.05	322°	−22°	3.69%	25.9	39	$1.51^{+0.26}_{-0.23}$	$+2.4\sigma$	2.20
63 EeV	295	163°	−3°	9.56%	26.3	46	$1.75^{+0.30}_{-0.26}$	$+3.3\sigma$	2.54	223°	+26°	9.56%	26.7	42	$1.57^{+0.28}_{-0.25}$	$+2.6\sigma$	2.31

flux of the highest-energy cosmic rays along this plane would not be completely unexpected, given that propagation lengths at the highest energies are limited to a few hundred megaparsecs—or even less, in the case of intermediate-mass nuclei (D. Allard 2012). On the other hand, UHECRs can undergo substantial deflections by Galactic and possibly intergalactic magnetic fields (M. S. Pshirkov et al. 2013; R. Alves Batista et al. 2017; M. Unger & G. R. Farrar 2024), preventing a one-to-one interpretation of arrival directions in terms of source positions.

Here, we use the intermediate angular scale of the aforementioned excess from the region reported in data from the Pierre Auger Observatory. As of the last update (Pierre Auger Collaboration 2023), the maximum local Li–Ma significance for a circular window was achieved with an energy threshold of $E_{\min} = 38$ EeV and a window radius of $\Psi = 27°$, whether the center of the window was constrained to be the position of Cen A or also scanned to avoid any assumption on the possible source location. In this work, we study whether other excesses with similar characteristics are present in different regions along the SGP, and/or at lower energies than previously studied. A search for excesses of events in bands centered around the SGP found no statistically significant result ($p = 0.13$ posttrial, Pierre Auger Collaboration 2022, Section 3.3), but a band in latitude may not capture an excess concentrated in a limited range of supergalactic longitude, hence in this work we consider top-hat windows (i.e., disk search regions) intersecting the SGP instead.

2. The Data Set

We use the same data set used in our last update on arrival directions (Pierre Auger Collaboration 2023) for searches for medium-scale anisotropies, namely events recorded using the surface detector (SD) array of the Pierre Auger Observatory from 2004 to 2022 inclusive. We only consider events with energies $E \geqslant 20$ EeV, as in Pierre Auger Collaboration (2018b). This is the same as the published data set of Pierre Auger Collaboration (2022) with the addition of the events detected in the years 2021 and 2022 and of events with energies 20 EeV $\leqslant E < 32$ EeV over the entire time period. As regards the last two years, only events detected by the parts of the array that had not yet undergone the AugerPrime upgrade (Pierre Auger Collaboration 2016) are used. As in Pierre Auger Collaboration (2022), we use all "vertical" events (with zenith angles $\theta < 60°$), in which the SD station with the largest signal is surrounded by at least four active stations and the reconstructed shower core is within an isosceles triangle of active stations, and all "inclined" events (with $60° \leqslant \theta < 80°$), in which the station closest to the reconstructed core position is surrounded by at least five active stations. The energies of these events are reconstructed with a total systematic uncertainty ∼14% and resolution ∼7%, and their arrival directions with a resolution <1°, for both vertical and inclined events. The total exposure of this data set is 135,000 km^2 sr yr.

As in Pierre Auger Collaboration (2022, 2023), the exposures to vertical and inclined events are rescaled so as to be proportional to the number of events in each zenith angle range (respectively, 6896 and 1936 above 20 EeV). We checked that the ratio between the number of inclined and vertical events, 0.281 ± 0.007, is within statistical uncertainties of the expectation 0.278 (Pierre Auger Collaboration 2022, Section 2 and Appendix A). The rescaling of exposures ensures that our analysis is very robust to any systematic effects affecting vertical and inclined events separately; we find that even artificially multiplying or dividing all inclined energies by a factor 1.25 before the rescaling would affect the resulting flux in the circular regions of the southern sky listed in Table 1 by less than the statistical uncertainties. By combining both zenith angle ranges ($0° \leqslant \theta < 80°$), the field of view (FOV) of the SD array covers all declinations $-90° \leqslant \delta < +44.8°$.

3. Analysis Method

In this work, for each of the six different energy thresholds, $E_{\min} = 20, 25, 32, 40, 50, 63$ EeV (i.e., $10^{19.3,19.4,\ldots,19.8}$ eV rounded to the nearest EeV), we consider all circular windows with radius $\Psi = 27°$ (the maximum-significance radius in Pierre Auger Collaboration 2023) centered on the positions on a HEALPix[104] grid (K. M. Górski et al. 2005) with $N_{\text{side}} = 2^6$ (resolution ≈0.9°) simultaneously meeting two criteria: first, we require that the SGP intersects the window, i.e., that the supergalactic latitude B of the window center satisfies $-\Psi \leqslant B \leqslant \Psi$; and second, as in our previous works, in order to have reasonably large statistics, we require that the center of the window be inside the FOV of the observatory, i.e., that the decl. of the window center satisfies $\delta < +44.8°$.[105] For each such window, we counted the numbers N_{in}, N_{out} of events in our data set with $E \geqslant E_{\min}$, respectively, inside the window and in the rest of the FOV, and computed the exposures $\mathcal{E}_{\text{in}}$, $\mathcal{E}_{\text{out}}$ by numerically integrating the expression in P. Sommers (2001, Section 2). From these, we computed the background number of events N_{bg} as $N_{\text{out}}\mathcal{E}_{\text{in}}/\mathcal{E}_{\text{out}}$, and the flux ratio $\Phi_{\text{in}}/\Phi_{\text{out}}$ as $N_{\text{in}}/N_{\text{bg}}$ (see Section 3.1).

[104] https://healpix.sourceforge.io/

[105] Note that this is slightly more conservative than the recommendation by T.-P. Li & Y.-Q. Ma (1983) that $N_{\text{in}} \gtrsim 10$ and $N_{\text{out}} \gtrsim 10$ when using the lowest of the energy thresholds we use here but slightly less conservative using the highest thresholds, i.e., some of the windows with centers closest to the edge of the FOV have $N_{\text{in}} \lesssim 10$ when using the highest thresholds.

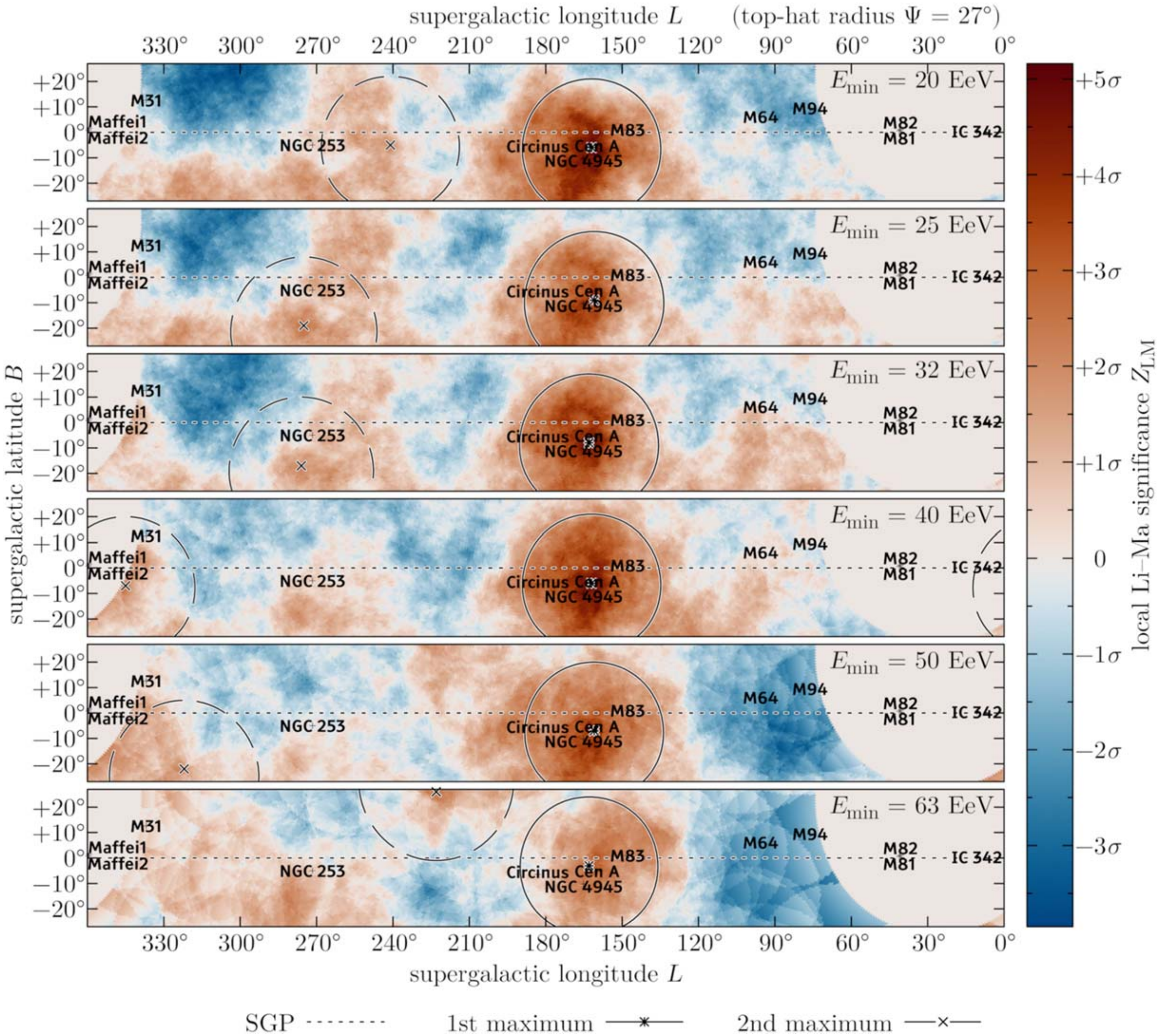

Figure 1. Local Li–Ma significance Z_{LM} of excesses over the isotropic expectation as a function of the window center position. The Z_{LM} in windows whose centers lie outside the FOV of the observatory was not computed (shown as the gray disk wrapping around the left and right edges of each panel; see also Figure 3). In each panel, the energy threshold used is written in the upper-right corner. The solid circle is the window position with the highest Z_{LM} in the whole strip; the dashed one is that with the highest Z_{LM} excluding those overlapping with the solid one. Labels indicate the position of Council of Giants galaxies (M. L. McCall 2014) for reference only; they are not taken into account in the analysis in any way.

3.1. Binomial Probability, Likelihood, and Upper Limit

For a given value of the ratio $\Phi_{\text{in}}/\Phi_{\text{out}}$ between the flux inside the window and that in the rest of the FOV (the isotropic null hypothesis being $\Phi_{\text{in}}/\Phi_{\text{out}} = 1$) and total number $N_{\text{tot}} = N_{\text{in}} + N_{\text{out}}$ of events above the energy threshold, the probability to observe exactly N_{in} events inside the window is

$$P\left(N_{\text{in}} \,\middle|\, N_{\text{tot}}, \frac{\Phi_{\text{in}}}{\Phi_{\text{out}}}\right) = \binom{N_{\text{tot}}}{N_{\text{in}}} p^{N_{\text{in}}}(1-p)^{N_{\text{tot}}-N_{\text{in}}}, \quad (1)$$

where

$$p = \frac{\Phi_{\text{in}}\mathcal{E}_{\text{in}}}{\Phi_{\text{in}}\mathcal{E}_{\text{in}} + \Phi_{\text{out}}\mathcal{E}_{\text{out}}} \quad (2)$$

is the probability for each event to fall within the window. This probability as a function of $\Phi_{\text{in}}/\Phi_{\text{out}}$ for a fixed N_{in}, N_{out} defines a likelihood function,

$$L(\Phi_{\text{in}}/\Phi_{\text{out}}) = P(N_{\text{in}}\,|N_{\text{tot}}, \Phi_{\text{in}}/\Phi_{\text{out}}), \quad (3)$$

which achieves its maximum at $\Phi_{\text{in}}/\Phi_{\text{out}} = \frac{N_{\text{in}}/\mathcal{E}_{\text{in}}}{N_{\text{out}}/\mathcal{E}_{\text{out}}} = N_{\text{in}}/N_{\text{bg}}$.

If we define the deviance (generalized χ^2, here with one degree of freedom) as

$$\begin{aligned} D(\Phi_{\text{in}}/\Phi_{\text{out}}) &= -2\ln\frac{L(\Phi_{\text{in}}/\Phi_{\text{out}})}{\max\limits_{\Phi_{\text{in}}/\Phi_{\text{out}}} L(\Phi_{\text{in}}/\Phi_{\text{out}})} \\ &= -2\ln\frac{L(\Phi_{\text{in}}/\Phi_{\text{out}})}{L(N_{\text{in}}/N_{\text{bg}})}, \end{aligned} \quad (4)$$

then $\pm\sqrt{D(\Phi_{\text{in}}/\Phi_{\text{out}})}$ is the number of standard deviations at which the data set disfavors a given value of $\Phi_{\text{in}}/\Phi_{\text{out}}$ with respect to the value $N_{\text{in}}/N_{\text{bg}}$; in particular, $\pm\sqrt{D(\Phi_{\text{in}}/\Phi_{\text{out}} = 1)}$ equals the local Li–Ma significance Z_{LM} (T.-P. Li & Y.-Q. Ma 1983).[106] The statistical uncertainties in $\Phi_{\text{in}}/\Phi_{\text{out}}$ we report in the tables are the $\pm 1\sigma$ intervals defined this way.

[106] The sign is + or − depending on whether $\Phi_{\text{in}}/\Phi_{\text{out}}$ is larger or smaller than the maximum-likelihood value $N_{\text{in}}/N_{\text{bg}}$.

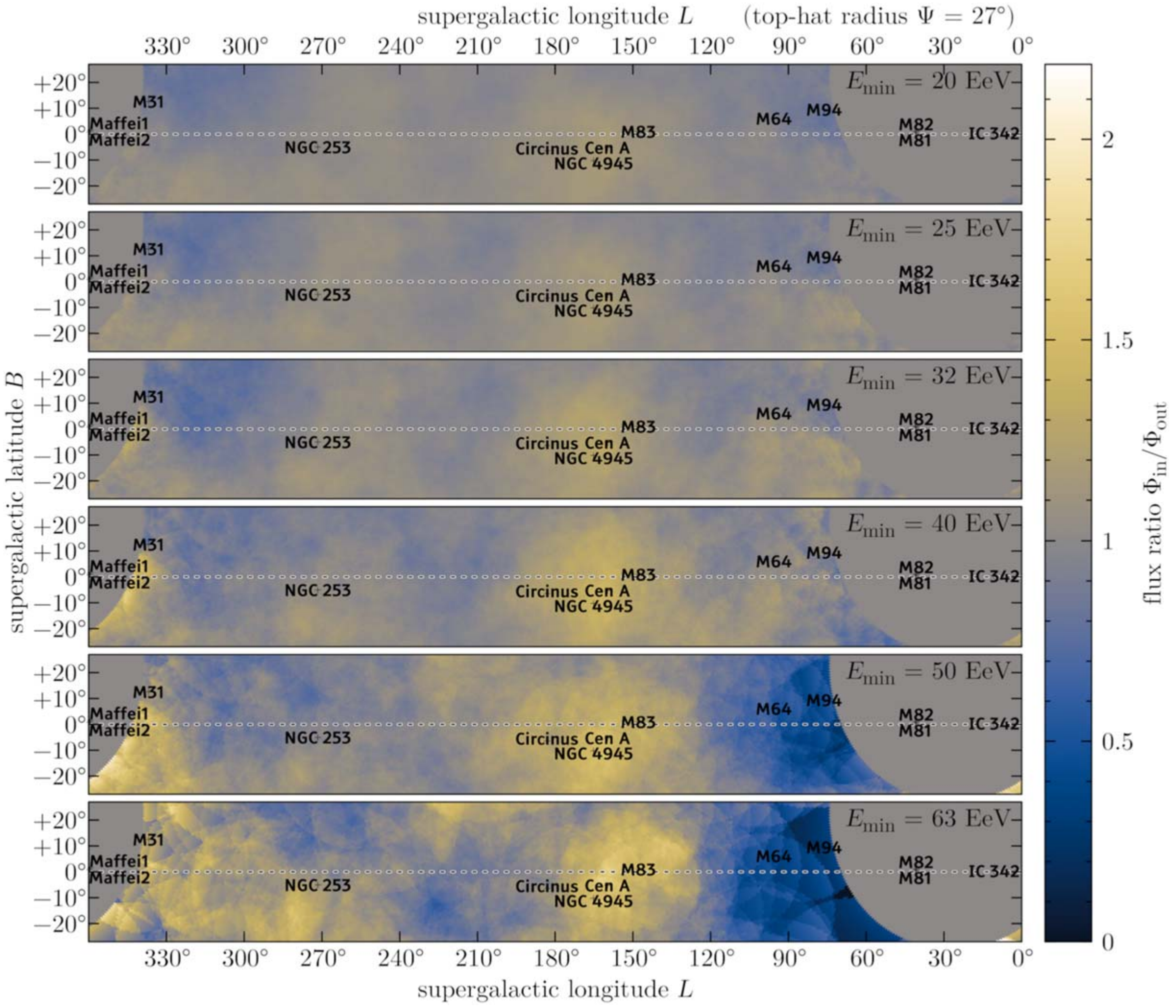

Figure 2. The maximum-likelihood value of the ratio $\Phi_{\rm in}/\Phi_{\rm out}$, i.e., $N_{\rm in}/N_{\rm bg}$, as a function of the window center position.

Finally, we define the frequentist 99% confidence level (CL) upper limit to $\Phi_{\rm in}/\Phi_{\rm out}$ as the $\Phi_{\rm in}/\Phi_{\rm out}$ value such that

$$\sum_{n=N_{\rm in}+1}^{N_{\rm tot}} P(n\,|N_{\rm tot},\,\Phi_{\rm in}/\Phi_{\rm out}) = 0.01; \tag{5}$$

in the cases we report, this agrees with the value such that $\sqrt{D(\Phi_{\rm in}/\Phi_{\rm out})} = 2.33$ to within a few percent.

4. Results

The local Li–Ma significance $Z_{\rm LM}$ as a function of the position of the window center in supergalactic coordinates (L, B) is shown in Figure 1, and the information about the window with the highest $Z_{\rm LM}$ for each $E_{\min}$ is provided in Table 1. We also search for the highest $Z_{\rm LM}$ among windows that do not overlap with the global maximum one (distance between centers $>2\Psi$). In Figure 2, we show the flux ratio $\Phi_{\rm in}/\Phi_{\rm out}$ computed as $N_{\rm in}/N_{\rm bg}$ as a function of the position of the window center.

4.1. Indication of an Excess in the Centaurus Region

As shown in the left part of Table 1 and by the solid circles in Figure 1, with all energy thresholds the most significant excess is the previously reported one in the Centaurus region. Its position is remarkably stable at least over a range of energy thresholds spanning half an order of magnitude (and of cumulative UHECR flux values spanning 1.5 orders of magnitude), with no discernible change in the maximum-significance window center. On the other hand, the strength $\Phi_{\rm in}/\Phi_{\rm out}$ of the excess does grow with the energy threshold, implying that the particles making up the excess have a different energy spectrum than the background, with a slower decrease with energy. By studying the number of events in this region in separate energy bins (see Appendix A for details), we find that the excess has a spectral index $\gamma = 2.6 \pm 0.3$. For comparison, the overall spectrum in our FOV (Pierre Auger Collaboration 2020b, with stricter quality cuts and a different reconstruction) has $\gamma = 3.05 \pm 0.05 \pm 0.10$ below $(46 \pm 3 \pm 6)$ EeV and $\gamma = 5.1 \pm 0.3 \pm 0.1$ above, where the first uncertainty is statistical and the second is systematic.

The local significance of $+5.2\sigma$ we find in the Centaurus region using the lowest energy threshold is exceeded for at least one of the window positions and energy thresholds in 912 out of 10^6 isotropic simulations, corresponding to a 3.1σ posttrial significance.

4.2. Study of TA-reported Excess Regions

As shown in the right part of Table 1 and by the dashed circles in Figure 1, the local significances of excesses in windows not overlapping with the maximum significance one are below 2.7σ for all the energy thresholds we tested. As shown in Appendix B,

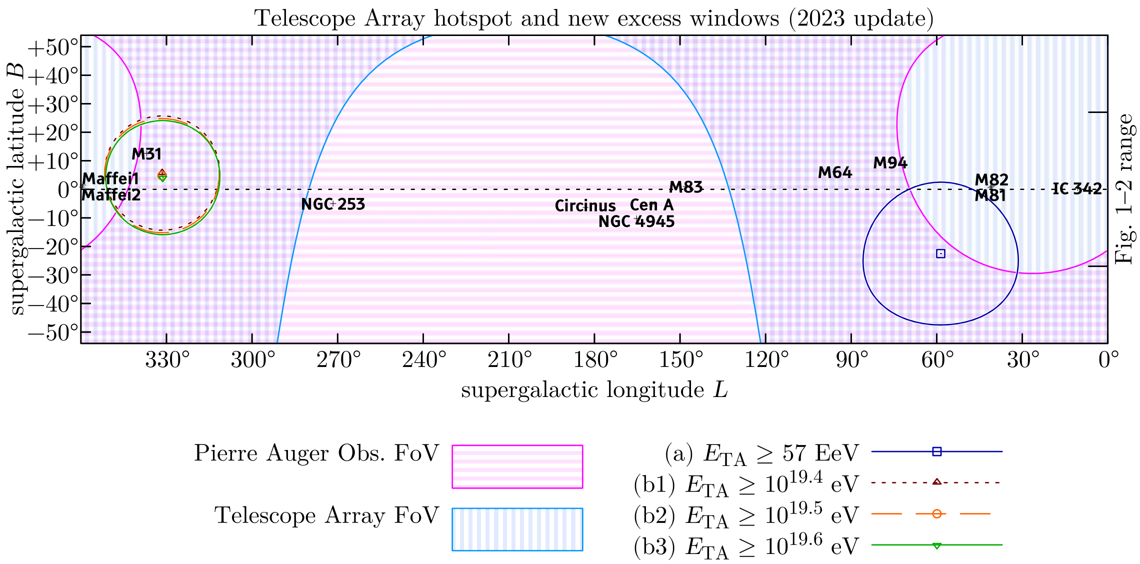

Figure 3. The windows in which the Telescope Array Collaboration reported excesses of events, as of their latest update (Telescope Array Collaboration 2023), compared to the FOV of the Pierre Auger Observatory and the TA.

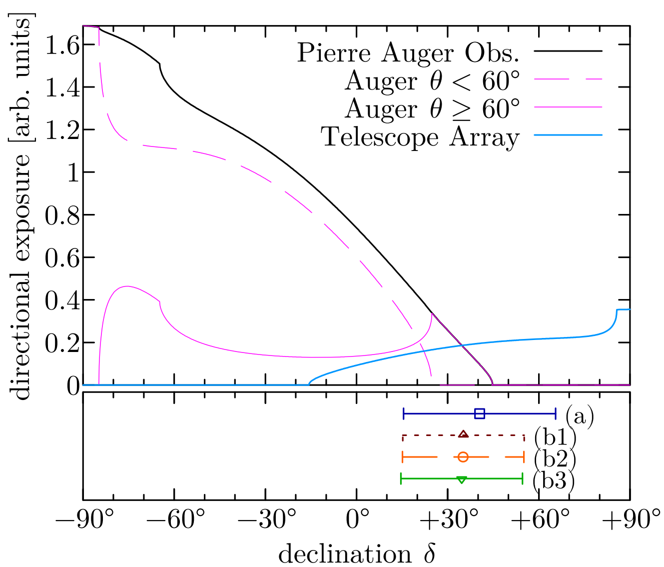

Figure 4. The directional exposure of the Pierre Auger Observatory and the TA as a function of decl., compared to the declinations of the windows shown in Figure 3 (horizontal bars; note that the bar lengths denote the sizes of the windows, not the uncertainties in their position).

this sets stringent upper limits on the flux, except very close to the edge of our FOV. The nonobservation of other excesses at this angular scale appears to contradict the reports by the Telescope Array Collaboration of an excess of cosmic rays with energies $E \geqslant 57$ EeV from a circular window (hereafter "TA hotspot") around $(\alpha, \delta) \approx (145°, +40°)$ (Telescope Array Collaboration 2014) and later of a weaker excess of events with $E \geqslant 10^{19.4,19.5,19.6}$ eV from a window around $(\alpha, \delta) \approx (20°, +35°)$ (Telescope Array Collaboration 2021b), both shown in Figure 3.

These reports have global statistical significances $\sim 3\sigma$ so far (as of Telescope Array Collaboration 2023), but nevertheless they have already been met with considerable interest in the community and spurred several attempts at phenomenological interpretations (e.g., L. A. Anchordoqui 2023; A. Neronov et al. 2023; P. Plotko et al. 2023).

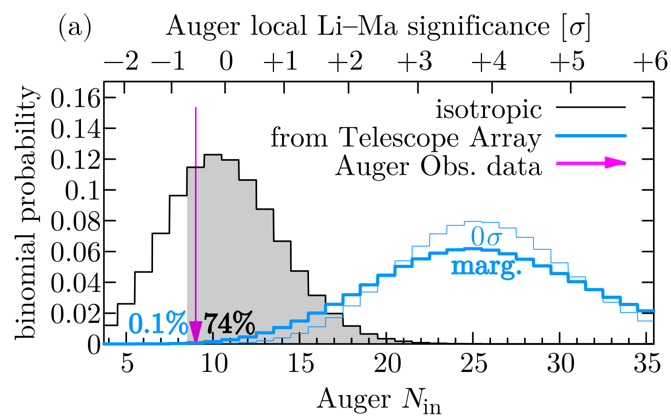

Figure 5. Binomial probability that N_{in} events would be observed in our data set in the first (a) of the windows reported by the TA and shown in Figure 3. The thin blue histogram assumes that the value of the flux ratio Φ_{in}/Φ_{out} is exactly the one reported by the TA, whereas the thick one is the marginal distribution of Φ_{in}/Φ_{out} over TA statistical uncertainties.

(The complete figure set (4 images) is available in the online article.)

Since these windows intersect the SGP and their centers are inside the FOV of the Auger Observatory (see also Figure 4), they are among the range of window centers we considered. As shown in Figure 1, we do not find any excesses at these positions when using comparable energy thresholds.

To find out what we could have expected to observe in our data given those reports from the TA, after correcting the energy thresholds for the known mismatch between the energy scales of the two observatories (Pierre Auger Collaboration & Telescope Array Collaboration 2023b, Equation (1)), we computed the distribution of the number N_{in} of events in our data set expected in each of these windows based on (i) isotropy ($\Phi_{in}/\Phi_{out} = 1$), (ii) the TA value of Φ_{in}/Φ_{out} that can be computed from their numbers of events N_{in}, N_{tot} as reported in their last update (Telescope Array Collaboration 2023), or (iii) the marginal distribution of Φ_{in}/Φ_{out} over TA statistical uncertainties. As we show in Figure 5, in each case we find that, based on the TA result, we would expect on average a local Li–Ma significance in our data of the order of 4σ,

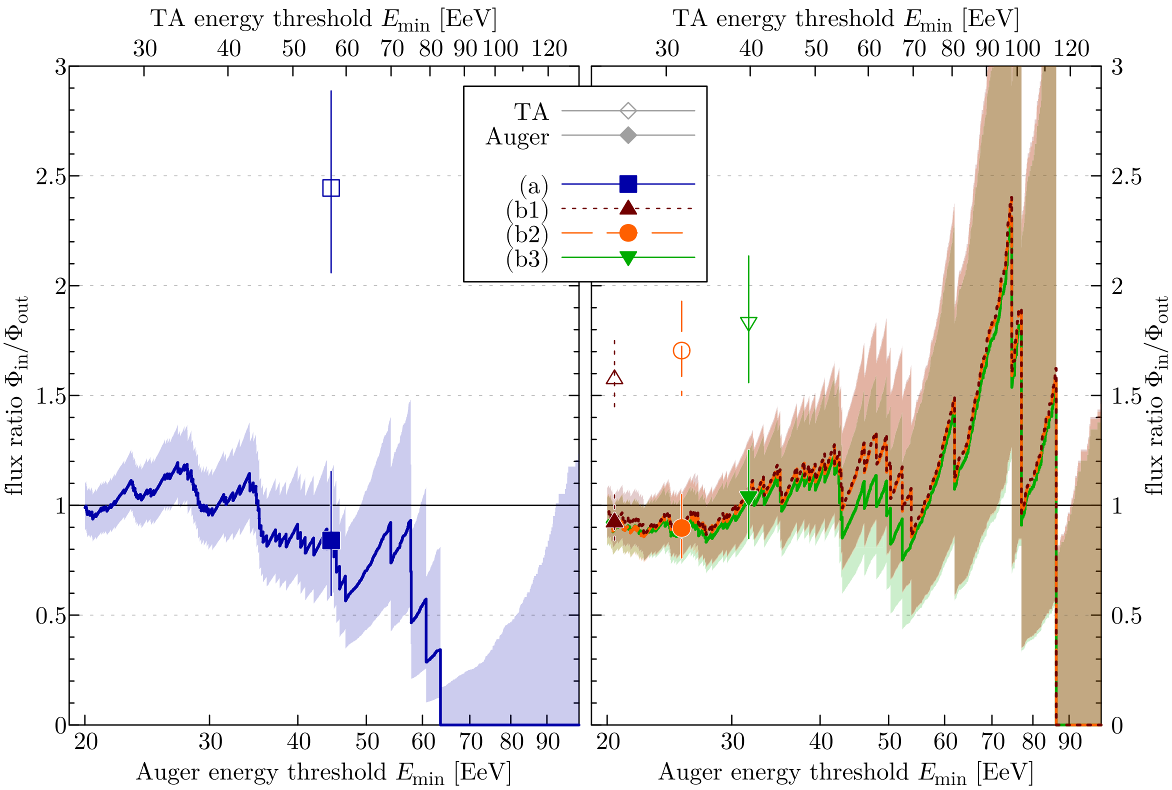

Figure 6. Flux ratio in the windows considered in this work (a, b1, b2, b3) computed from our data with all possible energy thresholds. The shaded bands show the $\pm 1\sigma$ interval for each threshold. The filled markers indicate the values at the thresholds computed via Pierre Auger Collaboration & Telescope Array Collaboration (2023b, Equation (1)); the uncertainties on the energy cross calibration are comparable to the horizontal size of the markers. The results reported in Telescope Array Collaboration (2023) are also shown as empty markers for comparison.

Table 2
The Excesses Reported by the TA in the Windows Shown in Figure 3, as of Their Latest Update (Telescope Array Collaboration 2023), and the Corresponding Results in Our Data

	TA (Telescope Array Collaboration 2023)									Pierre Auger Observatory (This Work)							
	E_{min}	N_{tot}	$\frac{\mathcal{E}_{in}}{\mathcal{E}_{tot}}$	N_{bg}	N_{in}	$\frac{\Phi_{in}}{\Phi_{out}}$	Z_{LM}	99% L.L.	post-trial	E_{min}	N_{tot}	$\frac{\mathcal{E}_{in}}{\mathcal{E}_{tot}}$	N_{bg}	N_{in}	$\frac{\Phi_{in}}{\Phi_{out}}$	Z_{LM}	99% U.L.
(a)	57 EeV	216	9.47%	18.0	44	$2.44^{+0.44}_{-0.39}$	$+4.8\sigma$	1.60	2.8σ	44.6 EeV	1074	1.00%	10.7	9	$0.84^{+0.31}_{-0.25}$	-0.5σ	1.76
(b1)	$10^{19.4}$ eV	1125	5.88%	64.0	101	$1.58^{+0.17}_{-0.16}$	$+4.1\sigma$	1.22	3.3σ	20.5 EeV	8374	0.84%	70.1	65	$0.93^{+0.12}_{-0.11}$	-0.6σ	1.23
(b2)	$10^{19.5}$ eV	728	5.87%	41.1	70	$1.70^{+0.22}_{-0.20}$	$+4.0\sigma$	1.25	3.2σ	25.5 EeV	5156	0.84%	43.5	39	$0.90^{+0.15}_{-0.14}$	-0.7σ	1.29
(b3)	$10^{19.6}$ eV	441	5.84%	24.6	45	$1.83^{+0.31}_{-0.27}$	$+3.6\sigma$	1.23	3.0σ	31.7 EeV	2990	0.87%	26.0	27	$1.04^{+0.21}_{-0.19}$	$+0.2\sigma$	1.61

Note. The E_{min} values are converted from the TA energy scale to ours using Pierre Auger Collaboration & Telescope Array Collaboration (2023b, Equation (1)). Some of the TA values of N_{bg}, Φ_{in}/Φ_{out}, and/or Z_{LM} shown here differ by up to a few percent from those reported in Telescope Array Collaboration (2023), presumably because in that work $\mathcal{E}_{in}/\mathcal{E}_{tot}$ was estimated from a Monte Carlo simulation with 100,000 events (of which $\mathcal{O}(10^4)$ within the window, hence with fluctuations $\sim$1% in $\mathcal{E}_{in}$), whereas here we computed it by numerically integrating the expression in P. Sommers (2001, Section 2) over a HEALPix grid with $N_{side} = 2^{10}$ (resolution $\approx 0^{\circ}.06$). For the TA results, we computed the frequentist 99% CL lower limit to Φ_{in}/Φ_{out} defined analogously to (5) by $\sum_{n=0}^{N_{in}-1} P(n|N_{tot}, \Phi_{in}/\Phi_{out}) = 0.01$. Note that the TA posttrial significances were computed under the assumption that only excesses near the center of a presumed emitting structure (the Perseus–Pisces Supercluster) had been searched for.

comparable to the TA value—since the integrated exposures we have accumulated in these windows are comparable to TA ones, as shown by the N_{bg} values[107] in Table 2. Instead, what we actually obtain is always $-0.7\sigma \lesssim Z_{LM} < +0.2\sigma$, in excellent agreement with the isotropic null hypothesis. In all cases, there exist possible values of Φ_{in}/Φ_{out} that would be compatible with both the 99% CL lower limit from TA data and the 99% CL upper limit from our data, e.g., $1.60 < \Phi_{in}/\Phi_{out} < 1.76$ in (a).

Telescope Array Collaboration (2018a) reported a deficit of events in the same part of the sky as the TA hotspot and at immediately lower energies, so that in a search for anisotropies with an energy threshold lower than that of the hotspot they

[107] We cannot compute the absolute integral exposure of the TA within each window (in km^2 sr yr) to directly compare it with ours, as the Telescope Array Collaboration (2023) did not report the total exposure of the data set. (Pierre Auger Collaboration & Telescope Array Collaboration 2023b did, but a different TA data set with stricter selection criteria was used there.)

would partially cancel each other out. To take into account the possibility that Pierre Auger Collaboration & Telescope Array Collaboration (2023b, Equation (1)) under- or overestimates the energy on the Pierre Auger Observatory scale corresponding to a given energy on the TA because of statistical and systematic uncertainties in the fit, we also computed $\Phi_{\mathrm{in}}/\Phi_{\mathrm{out}}$ and Z_{LM} values with different energy thresholds, finding that no other choice of threshold yields significances comparable to what we would expect based on the TA results, either (Figure 6).

A limitation of this study is that the likelihood in Equation (3) implicitly assumes a constant UHECR flux Φ_{in} inside the window being considered and a constant flux Φ_{out} outside. Whereas the directional exposure of the TA is roughly uniform within the windows shown in Figure 3, that of the Pierre Auger Observatory steeply decreases with increasing decl. (and even vanishes in part of the windows), as shown in Figure 4, so a flux excess more concentrated in the northern than in the southern part of a window would on average be underestimated when using data from the Auger Observatory. On the other hand, it should be noted that the TA window positions were not fixed a priori, but chosen in order to maximize the statistical significance of the excesses using TA data. This indicates that the excess is located roughly equally in the northern and southern parts of the window: if more of the excess were in the northern than in the southern part of the window, the significance would have been maximized by a different window further north, and vice versa. Similar considerations could apply to a decl. dependence of the flux outside the window being considered, but in Pierre Auger Collaboration (2020b) we found that the flux of UHECRs does not appreciably vary with decl. within our FOV other than the dipole mentioned in Section 1. Furthermore, the decl. dependence in the TA FOV claimed in Telescope Array Collaboration (2018b, 2024), if anything, would make the TA overestimate and the Auger Observatory underestimate Φ_{out}, going in the opposite direction than what would explain away the difference between the $\Phi_{\mathrm{in}}/\Phi_{\mathrm{out}}$ values from the two data sets.

5. Discussion and Conclusions

We have confirmed our previous finding (Pierre Auger Collaboration 2023, with 4.0σ posttrial there) that the statistically most significant excess of UHECRs along the SGP is from the Centaurus region, though still not at the discovery level with the current statistics (posttrial significance 3.1σ for a fixed search radius in this work), and we have further found that this excess extends to lower energies than previously studied (down to 20 EeV), with no appreciable dependence of its position on the energy threshold chosen. In case future experiments with more statistics confirm this excess, one possible explanation for the lack of energy dependence of its position (other than the absence of sizable coherent magnetic deflections) could be an approximately constant magnetic rigidity $R = E/Z$ of the particles in it, i.e., an increasingly heavy mass composition such that their atomic numbers Z are proportional to their energy.

On the other hand, no statistically significant excesses were found in the regions where the TA reported excesses of events, despite comparable integral exposures in those regions. It will be interesting to see whether the AugerPrime (Pierre Auger Collaboration 2016) and TA $\times$ 4 (Telescope Array Collaboration 2021a) upgraded detectors or future observatories such as GRAND (GRAND Collaboration 2020), POEMMA (POEMMA Collaboration 2021), or GCOS (GCOS Collaboration 2023) will confirm or rule out the indications for excesses reported by current experiments, and/or detect other anisotropies too weak to be noticed with the number of events gathered so far by current observatories. If any excesses are confirmed, event-by-event mass information from upgraded detectors (Pierre Auger Collaboration 2016) and/or machine learning techniques (Telescope Array Collaboration 2019; Pierre Auger Collaboration 2021a, 2021b) will help us elucidate their origin in the future by examining whether and how the mass composition in such regions differs from that in the rest of the sky and the energy dependence of any such differences.

Acknowledgments

The successful installation, commissioning, and operation of the Pierre Auger Observatory would not have been possible without the strong commitment and effort from the technical and administrative staff in Malargüe. We are very grateful to the following agencies and organizations for financial support:

Argentina—Comisión Nacional de Energía Atómica; Agencia Nacional de Promoción Científica y Tecnológica (ANPCyT); Consejo Nacional de Investigaciones Científicas y Técnicas (CONICET); Gobierno de la Provincia de Mendoza; Municipalidad de Malargüe; NDM Holdings and Valle Las Leñas, in gratitude for their continuing cooperation over land access; Australia—the Australian Research Council; Belgium—Fonds de la Recherche Scientifique (FNRS); Research Foundation Flanders (FWO), Marie Curie Action of the European Union grant No. 101107047; Brazil–Conselho Nacional de Desenvolvimento Científico e Tecnológico (CNPq); Financiadora de Estudos e Projetos (FINEP); Fundação de Amparo à Pesquisa do Estado de Rio de Janeiro (FAPERJ); São Paulo Research Foundation (FAPESP) grant Nos. 2019/10151-2, 2010/07359-6, and 1999/05404-3; Ministério da Ciência, Tecnologia, Inovações e Comunicações (MCTIC); Czech Republic—GACR 24-13049S, CAS LQ100102401, MEYS LM2023032, CZ.02.1.01/0.0/0.0/16_013/0001402, CZ.02.1.01/0.0/0.0/18_046/0016010, CZ.02.1.01/0.0/0.0/17_049/0008422, and CZ.02.01.01/00/22_008/0004632; France—Centre de Calcul IN2P3/CNRS; Centre National de la Recherche Scientifique (CNRS); Conseil Régional Ile-de-France; Département Physique Nucléaire et Corpusculaire (PNC-IN2P3/CNRS); Département Sciences de l'Univers (SDU-INSU/CNRS); Institut Lagrange de Paris (ILP) grant No. LABEX ANR-10-LABX-63 within the Investissements d'Avenir Program grant No. ANR-11-IDEX-0004-02; Germany—Bundesministerium für Bildung und Forschung (BMBF); Deutsche Forschungsgemeinschaft (DFG); Finanzministerium Baden-Württemberg; Helmholtz Alliance for Astroparticle Physics (HAP); Helmholtz-Gemeinschaft Deutscher Forschungszentren (HGF); Ministerium für Kultur und Wissenschaft des Landes Nordrhein-Westfalen; Ministerium für Wissenschaft, Forschung und Kunst des Landes Baden-Württemberg; Italy—Istituto Nazionale di Fisica Nucleare (INFN); Istituto Nazionale di Astrofisica (INAF); Ministero dell'Università e della Ricerca (MUR); CETEMPS Center of Excellence; Ministero degli Affari Esteri (MAE), ICSC Centro Nazionale di Ricerca in High Performance Computing, Big Data, and Quantum

Computing, funded by European Union NextGenerationEU, reference code CN_00000013; México—Consejo Nacional de Ciencia y Tecnología (CONACYT) No. 167733; Universidad Nacional Autónoma de México (UNAM); PAPIIT DGAPA-UNAM; The Netherlands—Ministry of Education, Culture, and Science; Netherlands Organization for Scientific Research (NWO); Dutch national e-infrastructure with the support of SURF Cooperative; Poland—Ministry of Education and Science, grant Nos. DIR/WK/2018/11 and 2022/WK/12; National Science Centre, grant Nos. 2016/22/M/ST9/00198, 2016/23/B/ST9/01635, 2020/39/B/ST9/01398, and 2022/45/B/ST9/02163; Portugal—Portuguese national funds and FEDER funds within Programa Operacional Factores de Competitividade through Fundação para a Ciência e a Tecnologia (COMPETE); Romania—Ministry of Research, Innovation and Digitization, CNCS-UEFISCDI, contract No. 30N/2023 under Romanian National Core Program LAPLAS VII, grant No. PN 23 21 01 02 and project No. PN-III-P1-1.1-TE-2021-0924/TE57/2022, within PNCDI III; Slovenia—Slovenian Research Agency, grants P1-0031, P1-0385, I0-0033, and N1-0111; Spain—Ministerio de Ciencia e Innovación/Agencia Estatal de Investigación (PID2019-105544GB-I00, PID2022-140510NB-I00, and RYC2019-027017-I), Xunta de Galicia (CIGUS Network of Research Centers, Consolidación 2021 GRC GI-2033, ED431C-2021/22, and ED431F-2022/15), Junta de Andalucía (SOMM17/6104/UGR and P18-FR-4314), and the European Union (Marie Sklodowska-Curie 101065027 and ERDF); USA—Department of Energy, contract Nos. DE-AC02-07CH11359, DE-FR02-04ER41300, DE-FG02-99ER41107, and DE-SC0011689; National Science Foundation, grant No. 0450696; The Grainger Foundation; Marie Curie-IRSES/EPLANET; European Particle Physics Latin American Network; and UNESCO.

Appendix A
Results Using Separate Energy Bins

In order to describe the energy dependence of the excess in the Centaurus region, we computed N_{in}, N_{bg}, and Z_{LM} in separate bins [20 EeV, 25 EeV), …, [50 EeV, 63 EeV), [63 EeV, $+\infty$) rather than cumulative ones [20 EeV, $+\infty$), [25 EeV, $+\infty$), …, keeping the window position fixed to the maximum significance one found in [20 EeV, $+\infty$). The results are listed in Table 3. Also, we fitted a power-law energy spectrum $\frac{dN}{dE} \propto E^{-\gamma}$ integrated over the bins to the excess $N_{\text{in}} - N_{\text{bg}}$, as shown in Figure 7. While the excess is considerably weaker in the third bin and barely present in the second bin, the behavior is still consistent with a simple power law with the current amount of statistics.

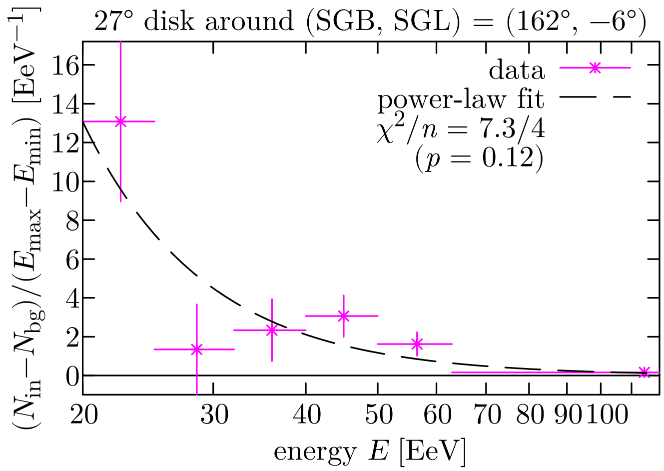

Figure 7. The number of excess events, $N_{\text{in}} - N_{\text{bg}}$, fitted as a power-law spectrum $N(E_{\text{min}}, E_{\text{max}}) = \int_{E_{\text{min}}}^{E_{\text{max}}} J_{20}\left(\frac{E}{20\,\text{EeV}}\right)^{-\gamma} dE = N_{20}\frac{E_{\text{min}}^{1-\gamma} - E_{\text{max}}^{1-\gamma}}{(20\,\text{EeV})^{1-\gamma}}$. The uncertainty on each entry is the sum in quadrature of those on N_{in} and N_{bg}, computed as $\sqrt{N_{\text{in}}}$ and $\sqrt{N_{\text{out}}}\,\mathcal{E}_{\text{in}}/\mathcal{E}_{\text{out}}$, respectively. In the last bin, we use $E_{\text{max}} = 166$ EeV, the energy of the most energetic event. The best-fit parameter values we obtain are $N_{20} = 160 \pm 32$ and $\gamma = 2.63 \pm 0.35$. Unlike in Pierre Auger Collaboration (2020b), in this work we do not correct for energy resolution effects; we estimate that here their effect on the spectral index would be an order of magnitude less than the statistical uncertainty of the fit.

Table 3
The Same as Table 1, but Using a Fixed Window Position $(L, B) = (162°, -6°)$ and Separate Energy Bins

E_{min}	E_{max}	N_{tot}	N_{bg}	N_{in}	$\frac{\Phi_{\text{in}}}{\Phi_{\text{out}}}$	Z_{LM}
20 EeV	25 EeV	3452	324.	389	$1.20^{+0.07}_{-0.06}$	$+3.3\sigma$
25 EeV	32 EeV	2444	233.	242	$1.04^{+0.07}_{-0.07}$	$+0.6\sigma$
32 EeV	40 EeV	1403	132.	151	$1.14^{+0.10}_{-0.10}$	$+1.5\sigma$
40 EeV	50 EeV	820	75.4	106	$1.41^{+0.15}_{-0.14}$	$+3.1\sigma$
50 EeV	63 EeV	418	37.9	59	$1.56^{+0.23}_{-0.21}$	$+3.0\sigma$
63 EeV	$+\infty$	295	26.6	43	$1.62^{+0.28}_{-0.25}$	$+2.7\sigma$

Appendix B
Upper Limits as a Function of the Window Position

In Figure 8, we show the frequentist 99% CL upper limit to $\Phi_{\text{in}}/\Phi_{\text{out}}$, as determined from Equation (5) for each of the energy thresholds and window positions we considered, showing how our data can set stringent upper limits to the flux in the windows except very close to the edge of the FOV.

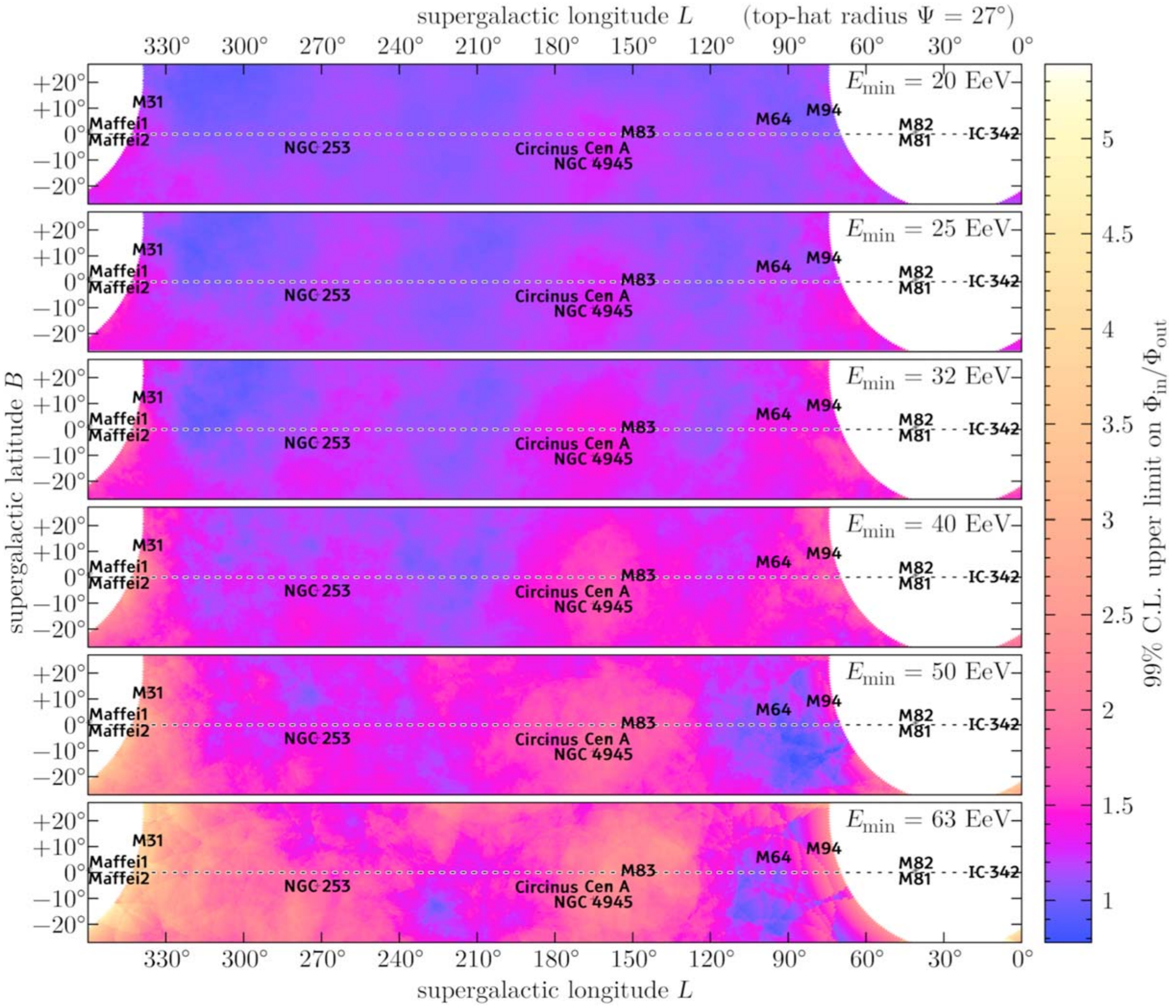

Figure 8. The same as Figure 1, showing the frequentist 99% CL upper limit to $\Phi_{\mathrm{in}}/\Phi_{\mathrm{out}}$ (Equation (5)).

ORCID iDs

T. Bister https://orcid.org/0000-0003-4005-0857
J. Biteau https://orcid.org/0000-0002-4202-8939
A. Bueno https://orcid.org/0000-0002-7439-4247
K.S. Caballero-Mora https://orcid.org/0000-0002-4042-3855
G. Cataldi https://orcid.org/0000-0001-8066-7718
A. Condorelli https://orcid.org/0000-0001-5681-0086
F. de Palma https://orcid.org/0000-0001-5898-2834
A. di Matteo https://orcid.org/0000-0002-8260-1867
C. Evoli https://orcid.org/0000-0002-6023-5253
H. Falcke https://orcid.org/0000-0002-2526-6724

References

Allard, D. 2012, APh, 39, 33
Alves Batista, R., Shin, M.-S., Devriendt, J., Semikoz, D., & Sigl, G. 2017, PhRvD, 96, 023010
Anchordoqui, L. A. 2023, PhRvD, 107, 083024
GCOS Collaboration 2023, PoS, 444, 281
Górski, K. M., Hivon, E., Banday, A. J., et al. 2005, ApJ, 622, 759
GRAND Collaboration 2020, SCPMA, 63, 219501
Li, T.-P., & Ma, Y.-Q. 1983, ApJ, 272, 317
McCall, M. L. 2014, MNRAS, 440, 405
Neronov, A., Semikoz, D., & Kalashev, O. 2023, PhRvD, 108, 103008
Pierre Auger Collaboration 2010, APh, 34, 314
Pierre Auger Collaboration 2016, arXiv:1604.03637
Pierre Auger Collaboration 2017, Sci, 357, 1266
Pierre Auger Collaboration 2018a, ApJ, 868, 4
Pierre Auger Collaboration 2018b, ApJL, 853, L29
Pierre Auger Collaboration 2020a, ApJ, 891, 142
Pierre Auger Collaboration 2020b, PhRvD, 102, 062005
Pierre Auger Collaboration 2021a, JInst, 16, P07016
Pierre Auger Collaboration 2021b, JInst, 16, P07019
Pierre Auger Collaboration 2022, ApJ, 935, 170
Pierre Auger Collaboration 2023, PoS, 444, 252
Pierre Auger Collaboration Telescope Array Collaboration 2023b, PoS, 444, 521
Plotko, P., van Vliet, A., Rodrigues, X., & Winter, W. 2023, ApJ, 953, 129
POEMMA Collaboration 2021, JCAP, 2021, 007
Pshirkov, M. S., Tinyakov, P. G., & Urban, F. U. 2013, MNRAS, 436, 2326
Sommers, P. 2001, APh, 14, 271
Telescope Array Collaboration 2014, ApJL, 790, L21
Telescope Array Collaboration 2018a, ApJ, 862, 91
Telescope Array Collaboration 2018b, arXiv:1801.07820
Telescope Array Collaboration 2019, PhRvD, 99, 022002
Telescope Array Collaboration 2021a, NIMPA, 1019, 165726
Telescope Array Collaboration 2021b, arXiv:2110.14827
Telescope Array Collaboration 2023, PoS, 444, 244
Telescope Array Collaboration 2024, arXiv:2406.08612
Unger, M., & Farrar, G. R. 2024, ApJ, 970, 95